Radiative Contributions Dominate Plasmon Broadening for Post-Transition Metals in the Ultraviolet

Maria V. Fonseca Guzman, Michael B. Ross*

Department of Chemistry, University of Massachusetts Lowell, Lowell, MA 01854

Keywords: Plasmonics, nanoparticles, UV, photonics, linewidth

Abstract

We use classical electrodynamics calculations to investigate the plasmonic properties of the post-transition metals Al, Bi, Ga, In, and Sn active in the ultraviolet, focusing in particular on the material- and resonance-dependent origins of plasmon broadening. Analytic Mie theory, the modified-long wavelength approximation, and the quasistatic dipole approximation together show that radiative processes dominate plasmon dephasing and damping in small (5-25 nm radius) Al, Bi, Ga, In, and Sn spheres. For Al, Ga, In, and Sn, the radiative contribution (~0.1–0.2 eV) to the plasmon linewidth is 10-fold greater than the non-radiative contribution (0.001–0.02 eV) from the bulk dielectric function. This is significantly different than what is observed for Ag spheres, where non-radiative contributions (~0.1 eV) are the primary source of broadening up to a radius of 25 nm. Overall, these data suggest that the plasmonic properties, dephasing, and lifetimes for Al, Ga, In, and Sn —and to a lesser extent Bi— spheres are qualitatively similar. These observations have important implications for the use of these metals for ultraviolet plasmonics. The increased

importance of radiative damping and dephasing processes for post-transition metals could influence the ability to harvest photons, generate hot carriers, and enhance spectroscopy in the ultraviolet while providing new opportunities for manipulating high-energy photons.

Introduction

Plasmonic metal nanoparticles have the remarkable ability to confine light into small volumes. This phenomenon is due to localized surface plasmon resonance (LSPR), the collective oscillation of conduction electrons. As a consequence of the LSPR, plasmonic nanoparticles strongly absorb and scatter light and enhance electric fields at their surface.[1] These properties have proven useful for applications in sensing, Raman spectroscopy enhancement, metamaterials, and catalysis.[2-6]

The majority of work in this field has focused on Ag and Au nanoparticles that are active in the visible and NIR regions due to their strong LSPRs and ease of synthesis. Recent efforts, however, have expanded plasmonic capabilities into the UV and min-infrared regions by focusing on a broader set of plasmonic materials.[7-9] The UV region is of particular interest because it presents opportunities for high-energy photon harvesting,[3] strongly enhanced spectroscopies due to resonance in organic molecules and polymers,[2, 10] and enhanced optical interactions with DNA and proteins.[11-14]

Continued progress in this area requires understanding the fundamental and material-dependent behavior for UV-active plasmonic materials. Numerous studies have determined the underlying photonic, electronic, and material-dependent mechanisms that determine the intensity and quality of the LSPR for Ag and Au.[7-8, 15-17] There is a less well-developed understanding of

these mechanisms in the subset of UV-active plasmonic metals, including Al, In, Sn, Ga, Bi, Rh, and Mg.[9, 18-25] Recent work suggests that Al nanoparticles have plasmonic behavior that is distinct from that typically seen for the noble metals, such that there are differences in the plasmon linewidth, dephasing, and lifetimes.[17, 26-30] Better understanding of the material-dependent plasmonic properties for the broader set of potential UV-plasmonic metals is important for their continued development and application.

Analysis of the LSPR linewidth is particularly useful for understanding the material-dependent plasmonic response. Using the plasmon linewidth, one can investigate the complex dephasing processes that describe how the LSPR decays into electron-hole pairs and phonons.[16-17, 31] While the linewidths are well-studied in Au and Ag, and to a lesser extent, Al, the material-dependent contributions to the LSPR for promising UV active metals, such as In, Sn, Ga, and Bi, have not been systematically deconstructed.[15-17, 26-28, 30-33] Doing so is essential for understanding which materials are most promising in the UV. Previous work has shown that the dephasing process is highly material dependent.[17] In general, there are two contributions to the plasmon linewidth and broadening, non-radiative and radiative. Radiative contributions describe interactions between photons emitted by the particle and the polarization of electrons within the particle. Non-radiative contributions describe intrinsic electronic transitions determined by the composition that are derived from the bulk dielectric function. In the noble metals, the plasmon quality and lifetime are dictated by a combination of radiative and non-radiative contributions for all particle sizes.[16-17] For Al, however, it was shown that radiative broadening dominates the LSPR in small spherical particles active in the 200-250 region.[17, 27] Understanding the contributions to the linewidth, specifically, the balance of radiative and non-radiative contributions, is essential for

designing UV plasmonic materials with efficient LSPRs, long plasmon lifetimes, and strongly enhanced near fields.

In this article, we explore the contributions to the plasmon linewidth in spherical Ag, Al, Bi, Ga, In, and Sn nanoparticles. Using generalized Mie theory, the modified long-wavelength approximation (MLWA), and the quasistatic approximation, we explore the size, linewidth, and material-dependent LSPR for these elements. We report that for small (5-25 nm radius) Sn, Al, In, Ga, and Bi spheres active in the UV, radiative contributions are the dominant broadening process for the LSPR. Specifically, radiative contributions account for >95% of the LSPR linewidth for all spherical Al, Ga, In, and Sn sizes considered (5-25 nm); this is in contrast to Ag nanoparticles of the same size, where non-radiative contributions are the primary contributor to the LSPR broadening. Because of this, we find the quasistatic approximation cannot accurately describe small Al, Sn, Bi, Ga, and In spheres due to the importance of field retardation effects at all sizes. The MLWA approximation, meanwhile, accurately describes the dipolar LSPR in spheres up to a radius of ~25 nm due to its ability to account for radiative damping and dynamic depolarization. For radii greater than 25 nm, Mie theory is required to account for multipolar resonances. Finally, we quantify the plasmonic quality factor and lifetimes for these elements and find that the post-transition metals Al, Ga, In, and Sn have similar plasmonic behavior while Bi is distinct throughout the UV and visible regions. When taken together, these data suggest that the Al, Bi, Ga, In, and Sn metals have intrinsically distinct LSPRs from Ag and Au in the visible due to the increased important of radiative broadening and relatively small non-radiative contributions in the UV. This has important implications for local field enhancement, the important of relative absorption to scattering, and the ability to utilize hot carriers.[34]

Materials and Methods

Quasistatic Dipole Approximation

For spheres that are small relative to the wavelength, the quasistatic dipole approximation provides a dipolar approximation for the LSPR. The induced dipole is given by[1]

$$\mathbf{P} = \alpha \mathbf{E} \text{ (1)}$$

Where **E** is the incident electromagnetic field and the polarizability of a sphere is given by[1]

$$\alpha = 4\pi \frac{\varepsilon - \varepsilon_b}{\varepsilon + 2\varepsilon_b} a^3 \text{ (2)}$$

Where ε is the complex frequency-dependent dielectric function, ε_b is the dielectric constant for the background media, and a is the radius of a sphere. Extinction is reported as an efficiency, determined by normalizing the extinction cross-section by the particle cross-section.

Modified Long-Wavelength Approximation (MLWA)

For spheres that are large relative to the wavelength, the radiative corrected field $\mathbf{E_{rad}}$ must be accounted for in Equation 1, such that[1]

$$\mathbf{P} = \alpha[\mathbf{E} + \mathbf{E_{rad}}] \text{ (3)}$$

Where $\mathbf{E_{rad}}$ is described by[1]

$$\mathbf{E_{rad}} = \frac{2}{3} ik^3 \mathbf{P} + \frac{k^2}{a} \mathbf{P} \text{ (4)}$$

Where k is the wavevector in the medium n given by $k = 2\pi n/\lambda$. The size-corrected dipole moment **P** can be determined by multiplying Equation 1 by[1]

$$g = \left[1 - \frac{2}{3} ik^3 \alpha - \frac{k^2}{a} \alpha\right]^{-1} \text{ (5)}$$

Here, the radiation damping term scales by k^3 and dynamic depolarization term scales by k^2. Extinction is reported as an efficiency, determined by normalizing the extinction cross-section by the particle cross-section.

Generalized Mie Theory

Mie theory calculations were used to calculate the optical response of spherical metal nanoparticles with a radius of 5-50 nm, 25 vector spherical harmonics were included for all calculations.[35] Dielectric functions were taken from the following references: Ag,[36] Al,[37] Ga,[38-39] In,[40] Bi,[41] and Sn[42]. Extinction, scattering, and absorption contributions are reported as optical efficiency, Q, which is a unitless quantity. Surface scattering was not accounted for because it was found to have a relatively small effect in previous work for Al,[27] and a background dielectric constant of 1 (vacuum) was used for all calculations.

Linewidth Fitting and Decomposition

The total homogeneous linewidth Γ_{total} is determined by fitting the dipolar extinction peak with the sum of Gaussian and Lorentzian functions, which helps account for peak asymmetry. This method works best for particles that do not exhibit higher-order resonances (*e.g.* quadrupoles), thus the values determined for the linewidths are limited by the particle radius at which a quadrupole is observed for each element.

The total linewidth is determined by the combination of the radiative and non-radiative contributions [15, 17]

$$\Gamma = \Gamma_{\text{radiative}} + \Gamma_{\text{non-radiative}} \quad (3)$$

where Γ is the linewidth of the LSPR based on Q_{ext},and $\Gamma_{\text{non-radiative}}$ is determined from the dielectric function according to [15-16]

$$\Gamma_{\text{non-radiative}} = \frac{2\text{Im}\{\varepsilon\}}{\sqrt{(\partial \text{Re}\{\varepsilon\}/\partial\omega)^2+(\partial \text{Im}\{\varepsilon\}/\partial\omega)^2}} \quad (4)$$

where $\Gamma_{\text{non-radiative}}$ is the linewidth associated with a dielectric function, $\Gamma_{\text{radiative}}$ is determined from $\Gamma_{\text{radiative}} = \Gamma - \Gamma_{\text{non-radiative}}$.

Results and Discussion

Optical Properties of Ag, Al, in, Sn, Ga, and Bi Spheres

Multiple levels of theory were used to investigate the optical properties of spheres with radii from 5-50 nm. Spherical nanoparticles were chosen due to their high energy LSPRs that can exist in the deep UV. **Figure 1** depicts the Mie theory calculated size-dependent extinction efficiency for Ag, Al, Bi, Ga, In, and Sn spheres. Al, Ga, In, and Sn support LSPRs well into the deep UV from 200-300 nm, Bi supports a broad LSPR 250-400 nm, and Ag supports an LSPR from 350-400 nm. The high energy onset of the LSPR is material-dependent and is determined by the dielectric function for each metal. While the analysis of the dielectric functions for these metals has been covered elsewhere,[7-8, 21] a comparison of the free electron density in these metals qualitatively illustrates why Al, Ga, In, Sn and Bi can support higher energy plasmonic resonances than Ag.

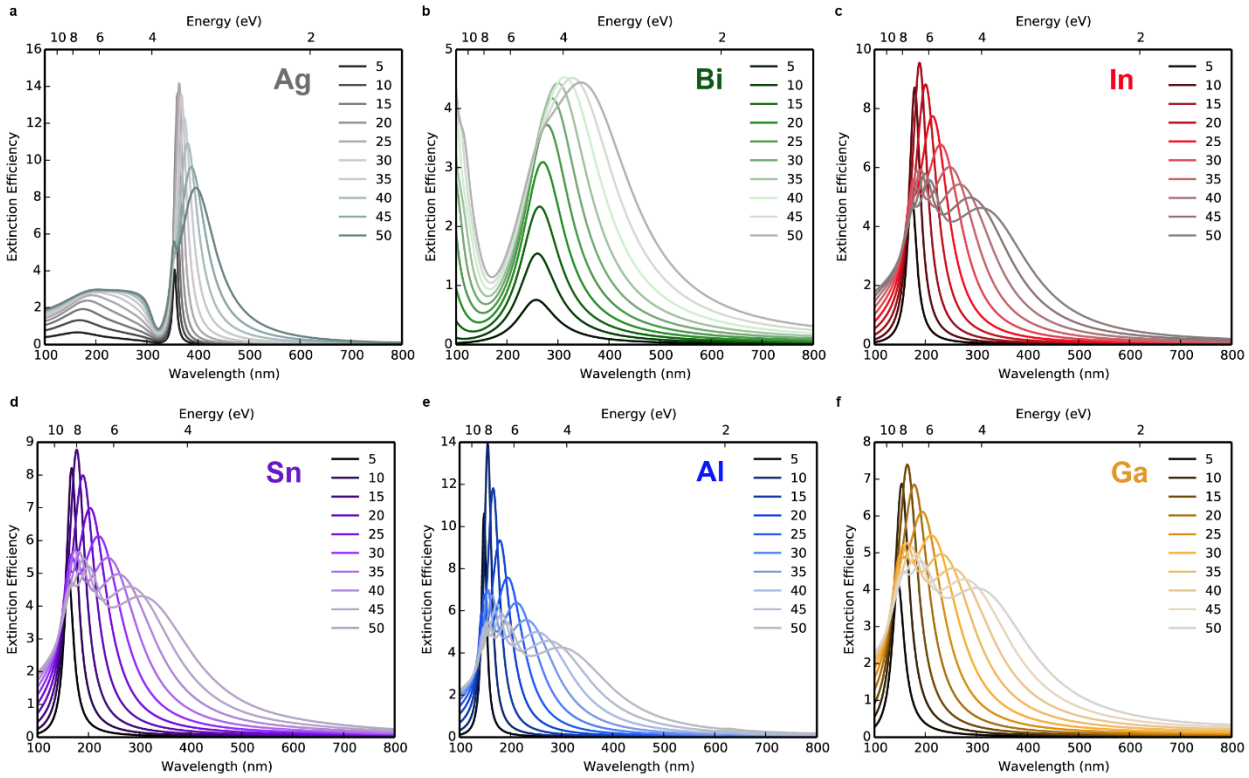

Figure 1. Simulated plasmonic response of Ag, Al, Ga, In, Bi, and Sn spheres. Extinction efficiencies calculated with Mie theory for 5–50 nm radius a) Ag, b) Al, c) Ga, d) In, e) Bi, and f) Sn spheres.

The particular characteristics of the dielectric function have complex physical origins, however, in the relatively simple Drude model the dispersion is largely determined by the plasma frequency, ω_p. The plasma frequency is directly dependent on the free electron density of a metal according to

$$\omega_p = \sqrt{\frac{Ne^2}{\varepsilon_0 m_e}} \quad (5)$$

where N is the number of free carriers, e is the charge of an electron, ε_0 is the permittivity of free space, and m_e is the electron mass. The plasma frequency determines the frequencies below (wavelengths above) which a metal can support a charge oscillation. Thus, while the particular characteristics of the dielectric function determine the complete plasmonic response, the onset of plasmonic activity correlates with the number of free carriers in the metal. By comparing the onset of the LSPR, *e.g.* for the 5 nm radius sphere, and the number of free carriers (**Table 1**),[43] the metals with the highest free electron density have the highest energy LSPR onset. While this relationship is well known and simplified here,[1, 7, 21] it highlights how the intrinsic physical properties of the post-transition metals Al, Ga, Sn, Bi, and In differentiate their plasmonic response from the more conventional noble metals.

Table 1. Electronic properties of metals in increasing order of free electron density.

Metal	**Free Electron Density, n (10^{22}/cm^3)**
Ag	5.86
In	11.5
Bi	14.1
Sn	14.8
Ga	15.4
Al	18.1

The Mie calculations show that the LSPR redshifts and broadens with an increasing radius for all metals. Additionally, beyond a material-dependent radius, multiple peaks are observed in the extinction spectra. These peaks correspond to higher-order modes e.g. quadrupolar, hexapolar, and octopolar resonances.[1, 27] These emerge due to the depolarization of the incident field across the volume of the particle; they emerge when the particle is significantly larger than the wavelength of light. Higher-order modes emerge on the higher energy side of the LSPR peak, for example, the quadrupole for In emerges at 180 nm for radii of 25 nm, while both a hexapole (180 nm) and quadrupole (210 nm) are present for sizes greater than 40 nm. Al, Ga, and Sn exhibit similar behavior. In contrast, Ag spheres with radii of 5 – 35 nm exhibit only a dipolar mode, with a quadrupole emerging at larger radii. Unlike the other metals, Bi only has a weak quadrupole that emerges at radii greater than ~ 40 nm.

For comparison with the analytic Mie results, both the quasistatic approximation and MLWA were used to simulate spheres of the same radius (**Figures S1 and S2**).[1, 44] These two levels of theory account for the size- and wavelength-dependence of the LSPR distinctly, and provide useful context for understanding the factors that determine plasmonic response. The quasistatic approximation is generally accurate when the wavelength of radiation is much larger than the particle size; it assumes that the particle is in a spatially uniform electrostatic field.[1, 44] For Al, Bi, Ga, In, and Sn, which have LSPRs below 260 nm, the quasistatic approximation does not correlate well to Mie Theory (**Figure S1**), while there is better agreement for Ag, which has an LSPR near 400 nm. This can be rationalized because for UV light, where the LSPR corresponds to a much shorter wavelength, the particle size is much close to the wavelength and thus the quasistatic approximation is less valid. For Ag, the quasistatic approximation is reasonably accurate for spheres with 5 – 30 nm radii while for Bi, spheres remain quasistatic up to 30 nm

radii. Above these radii, significant red-shifting and broadening of the LSPR is observed (**Figure 1**)..

To account for the red-shifting and broadening terms observed in the dipolar LSPR, we use MLWA, which includes radiative damping and dynamic depolarization effects (**Figure S2**).[1, 25, 45] Radiative damping is related to the spontaneous emission of photons due to the induced dipole. It has a strong dependence on the free electron density of a metal and the particle volume and it results primarily in damping and broadening.[1, 17] Dynamic depolarization is related to depolarization of the incident radiation across the particle and it results in the red shifting of the LSPR as the particle size increases. Because it can account for these two phenomena, the MLWA accurately describes the LSPR for all materials studied here up to the radius at which higher-order modes emerge **(Figure S2)**. Overall, the quasistatic and MLWA calculations suggest that size-dependent effects in the UV-active plasmonic nanoparticle are distinct from those in Ag, and that radiative contributions play a prominent role in the LSPR even for small spheres.

To better understand the measurable quantities that comprise the extinction spectrum, we can analyze the absorption and scattering efficiencies separately. **Figure 2** depicts the absorption efficiency over the same range of radii as **Figure 1**. In general, the absorption efficiency is narrower than the extinction and it does not exhibit significant red-shifting with increasing size. For Ag spheres, the absorption efficiency is greater (~10) than that of any other metal. While Al has a maximum absorbance efficiency approaching 10, this occurs for the smallest sphere (5 nm) and decreases rapidly with increasing size. Similar behavior is observed for Ga, In, and Sn. Previously this size-dependent behavior was ascribed to a red-shifting of the LSPR toward the lossier part of the dielectric function for Al, a similar explanation appears to be true for Ga, In, and Sn.[21, 27] Bi has the lowest absorption efficiency maximum for any of the metals investigated here.

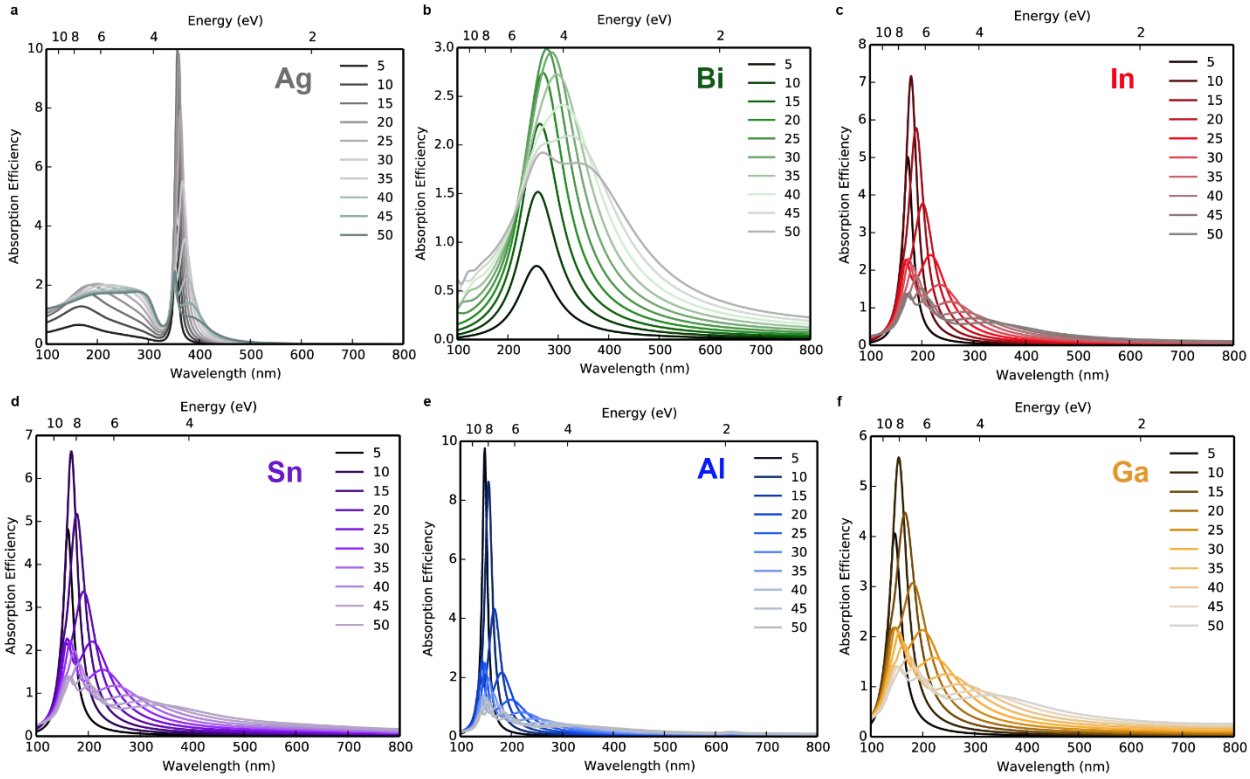

Figure 2. Calculated absorption for Ag, Al, Ga, In, Bi, and Sn spheres. Absorption efficiencies calculated with Mie theory for 5–50 nm radius a) Ag, b) Al, c) Ga, d) In, e) Bi, and f) Sn spheres.

By comparison with the absorption, the scattering efficiency is broadened, damped, and red-shifted (**Figure 3**). These changes are due to the same phenomena described by the MLWA, namely, radiative damping and dynamic depolarization.[1, 17] As anticipated, Al, Ga, In, and Sn exhibit similar behavior to the extinction spectra, such as broadened LSPRs for sphere radii exceeding 20 – 25 nm. The scattering efficiency exceeds the absorption efficiency in Al and Sn

for radii greater than 15 nm, in Ga and In for radii greater than 20 nm, in Ag for radii greater than 25 nm, and in Bi for radii greater than 35 nm. These data suggest that radiative and size-dependent broadening effects are significantly more pronounced in all of the UV-active materials investigated here, such that even at radii as small as 5 nm they are not well-described by the quasistatic dipole approximation. To better understand the contributions to broadening for the UV-resonant metals, it is necessary to investigate the specific linewidth contributions to the LSPR.

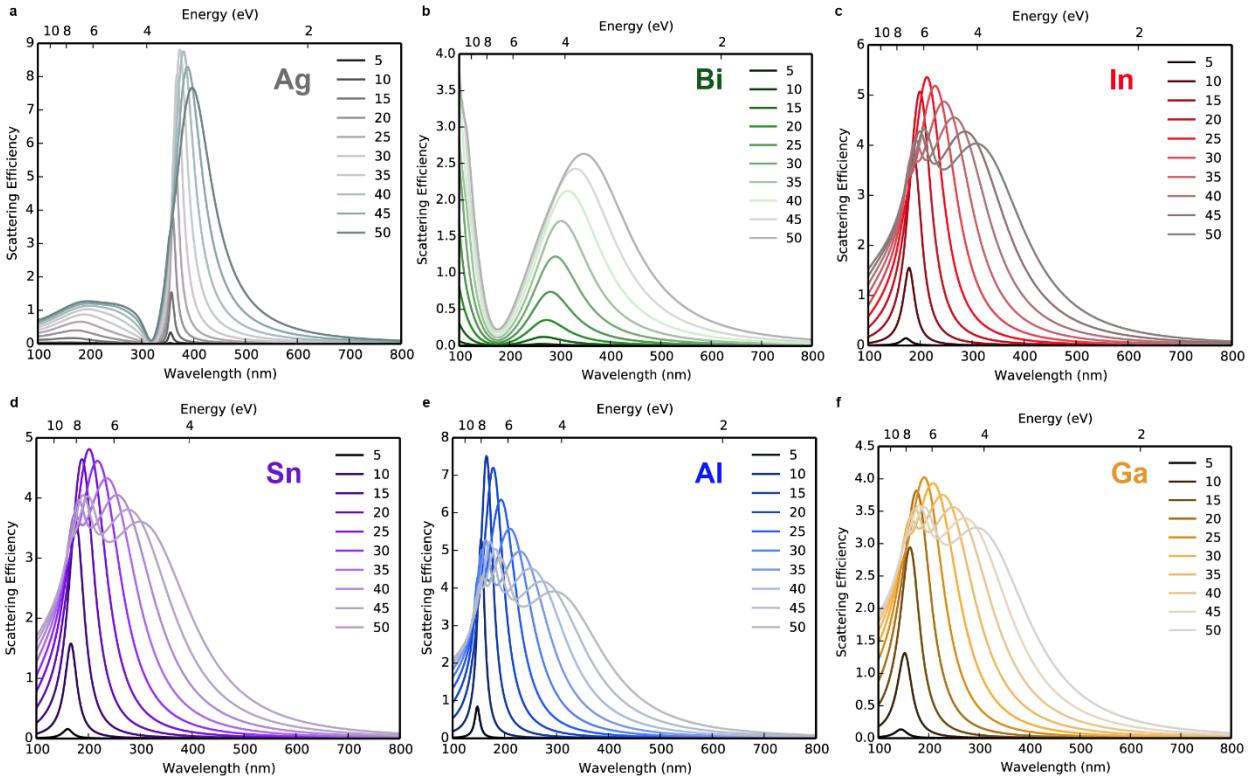

Figure 3. Calculated scattering for Ag, Al, Ga, In, Bi, and Sn spheres. Scattering efficiencies calculated with Mie theory for 5–50 nm radius a) Ag, b) Al, c) Ga, d) In, e) Bi, and f) Sn spheres.

Contributions to the Linewidth

The total linewidth is determined by fitting the peak of extinction efficiency and is defined as the full width at half maximum (FWHM) of the dipolar resonance (Methods). **Figure 4** shows the size-dependent values of the total linewidth Γ that are obtained from the fit of the extinction efficiency. As is well known, Ag has a narrow linewidth, nearly an order of magnitude less than the other metals. For example, for a 15 nm radius sphere, Al and In have linewidths of ~1.3 eV, while Ag has a linewidth of ~0.1 eV. Similarly, the linewidth is 1.5 and 2.2 eV for Sn and Ga, respectively. Among the UV active metals, Al exhibits the narrowest linewidth, however, the linewidths for In and Sn are similar (within 0.5 eV) for spheres with radii less than 15 nm.

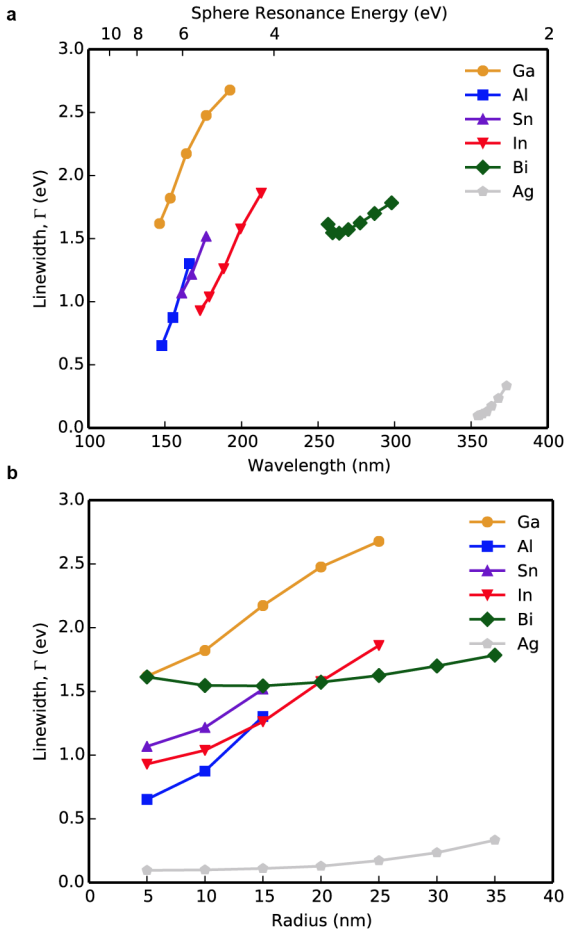

Figure 4. The plasmonic linewidth for Al, Ag, Bi, Ga, In, and Sn spheres. The homogeneous linewidth Γ for Al (blue squares), Ag (grey pentagons), Bi (green diamonds), Ga (orange circles), In (red nablas), and Sn (purple triangles) as a function of wavelength (a) and radius (b).

To better understand the origin of broadening of the linewidths, it is important to deconvolute the total linewidth into its non-radiative and radiative components (see Methods for more information).[15-17] Within the context of this work, deconvolution of the linewidth is important for quantifying the relative contribution of radiative effects that are related to the size-dependent broadening and lack of quasistatic behavior for Al, Ga, In, and Sn spheres. **Figure 5** depicts the deconvolution of the total linewidth Γ for Ag, Al, Bi, Ga, In, and Sn spheres. Here, the radiative contribution is the difference between the total linewidth and the non-radiative contribution taken at λ_{max}. For Ag, the primary contribution to Γ is non-radiative up to a radius of 30 nm, above which $\Gamma_{radiative}$ is a greater contributor. This is because the non-radiative contribution does not change significantly as a function of the radius due to the flat nature of the Ag dielectric function over this region while $\Gamma_{radiative}$ increases as a function of particle volume.[15, 27] In contrast, the linewidth contributions for Bi, In, Sn, Al, and Ga show that Γ is primarily composed of radiative broadening effects, with a small (<0.01 eV) non-radiative contribution. For Al, In, and Sn, $\Gamma_{non\text{-}radiative}$ — the intrinsic broadening due to the bulk dielectric function —is less than 0.01 eV, about an order of magnitude smaller than in Ag (~0.1 eV), while it is only ~ 0.2eV for Ga. This means that for Al, Ga, In, and Sn, $\Gamma_{radiative}$ is 10-fold greater than $\Gamma_{non\text{-}radiative}$, even for the smallest sphere radius investigated here (5 nm).

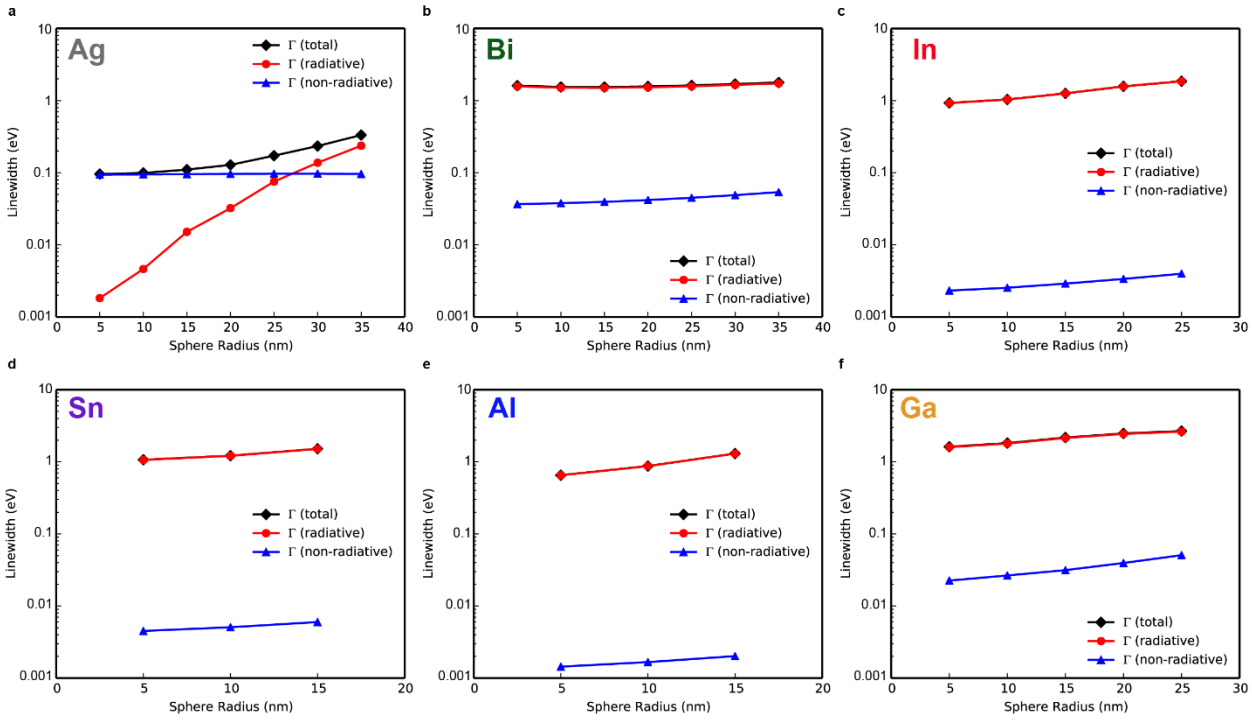

Figure 5. Contributions to the homogeneous linewidth Γ. Separation of the total linewidth Γ (black diamonds), radiative linewidth $\Gamma_{radiative}$ (red circles), and $\Gamma_{non\text{-}radiative}$ (blue triangles), for a) Ag, b) Bi, c) In, d) Sn, e) Al, and f) Ga.

We note that the MLWA captures these differences in the broadening contributions (**Figure S2)** by accounting for dynamic depolarization and radiative damping effects. In particular, this can be understood by the k^3 scaling of the radiation damping term in the modified polarizability, which is more pronounced at high energy LSPRs.[27] While the linewidth decomposition provides physical insight into the broadening mechanisms for the LSPR, it can also be related to quantities such as the quality factor and plasmon lifetime that are important for a variety of applications.

Quality Factors and Dephasing Times

While the plasmon linewidth and its contributions aid in gaining physical insight into the LSPR for different materials, quantities such as the plasmon quality factor and linewidth are of practical importance and provide context for applications. The quality factor of a resonance, defined as $Q = E_{\mathrm{LSPR}}/\Gamma$, describes the extent of local field enhancement and confinement of light.[30, 46] The highest quality factors are observed for Ag, 10 – 40, depending on the radius (**Figure 6a**). However, the Ag LSPR is limited to a small range in the visible region between 360 and 380 nm. In contrast, Al, Bi, Ga, In and Sn allow access to LSPRs over the broad range of UV wavelengths from 140-300 nm, depending on the material. However, these LSPRs do have lower quality factors than that observed for Ag. For example, Al exhibits quality factors of 6 – 13 in the range of 150 – 170 nm, while Sn and In quality factors are in the range of 4 – 8 in the range of 150 – 180 nm and 170 – 230 nm, respectively (**Figure 6a**).

The homogeneous linewidth was also used to calculate the dephasing times (T) which describe the time scale over which the plasmon oscillation is coherent.[16] These were determined according to the relation $T = 2\hbar/\Gamma$.[15] The dephasing time describes both radiative and non-radiative energy loss processes and measures the ability to support a perfectly coherent oscillation, where decoherence occurs due to radiation damping and non-radiative processes. In general, the LSPR dephasing time increases with size due to the effect of increasing particle volume on broadening (**Figure 6b**).[16-17] As expected, Ag shows the longest dephasing time of 14 fs. By comparison, the dephasing times for Al, Ga, In, and Sn are in the range from 1–2.5 fs, while Ga and Bi are both faster than 1 fs.

Overall the quality factor and plasmon dephasing times are easily compared for different metals and have significance in the LSPR lifetime and efficiency and magnitude of plasmon field enhancement. While Ag exhibits the highest quality resonances throughout the visible, Al, Ga, In, and Sn all exhibit reasonably high-quality plasmon resonances in the UV with plasmon lifetimes of at least 1 fs. Unlike the noble metals, these resonances are in the deep UV for small spherical nanoparticles. As discussed above, the primary contribution to LSPR broadening and damping for these post-transition metals is radiative (**Figure 6c**).

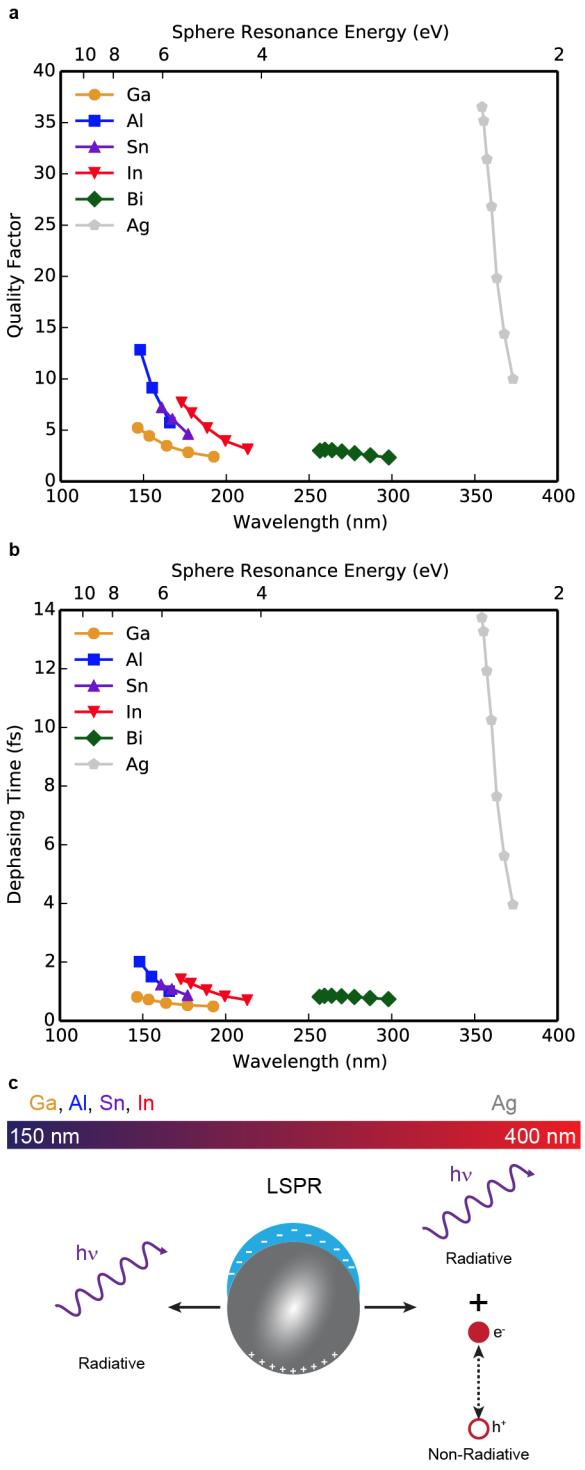

Figure 6 The plasmonic quality and lifetime. The calculated plasmon quality factor a) and lifetime (b) for Ga (orange circles), Al (blue squares), Sn (purple triangles), In (red nablas), Bi

(green diamonds), and Ag (grey pentagons). c) depicts the primary contributions and wavelengths for the plasmonic materials investigated in this work.

Conclusion

We have calculated the optical properties of spherical nanoparticles for metals with LSPRs throughout the UV. We find that radiative contributions dominate the plasmonic response for Al, Ga, In, Sn, and, to a lesser extent Bi, when compared to Ag. These results are consistent with previous investigations for Al and noble metal nanoparticles,[16-17, 27-28, 46] while demonstrating the significance of radiative effects other promising UV-active post-transition plasmonic metals (**Figure 6c)**. For the radii studied here (5-30 nm), the radiative contribution makes up a larger fraction than the non-radiative portion of the linewidth even spheres as small as 5 nm in radius. This is distinct from the behavior of Au and Ag, where non-radiative contributions dictate the linewidth for small spheres.[7, 16, 27] While there are relatively few experimental investigations for small In, Ga, and Sn spheres, the calculated optical spectra and quality factors for these metals suggest that their behavior would be qualitatively similar to Al in the UV.

These results have broad implications for designing functional plasmonic nanoparticles in the UV. The relative significance of radiative effects in small Al, Ga, In, and Sn spheres suggests that radiative damping and scattering contributions could be a challenge for plasmonic nanoparticles in the deep UV, however, there is evidence that Au dimers can still provide significant Raman enhancement even with significant radiative effects.[47] Furthermore, there are demonstrations that anisotropic or film-coupled Al nanoparticles can support high-quality LSPRs and overcome radiation damping pathways, similar possibilities likely exist for the other post-

transition metals investigated here.[28, 30, 48-49] This work demonstrates that the plasmon resonances for the post-transition metals Al, Bi, Ga, In and Sn in the UV are fundamentally different than those for the noble metal nanoparticles and that these materials are promising for new opportunities for UV optical enhancement.

Supporting Information

Quasistatic and modified-long wavelength approximation calculated spectra for Ag, Al, Bi, Ga, In, and Sn are included.

The Supporting Information is available free of charge on the ACS Publications website.

Author Information:

Corresponding Author:

Correspondence and requests for materials should be sent to M.B.R. (Michael_ross@uml.edu).

ORCID:

Michael B. Ross 0000-0002-2511-0594

Maria V. Fonseca Guzman 0000-0001-8931-1224

Author Contributions

All authors have given approval to the final version of the manuscript.

Conflicts of Interest

Notes:

The authors declare no competing financial interests.

Acknowledgments

This material was supported by the University of Massachusetts Lowell and the Commonwealth of Massachusetts. M.V.F.G. gratefully acknowledges support from the RIST Institute for Sustainability and Energy.

References

1. Kelly, K. L.; Coronado, E.; Zhao, L. L.; Schatz, G. C., The Optical Properties of Metal Nanoparticles: The Influence of Size, Shape, and Dielectric Environment. *The Journal of Physical Chemistry B* **2003**, *107*, 668-677.

2. Ben-Jaber, S.; Peveler, W. J.; Quesada-Cabrera, R.; Cortés, E.; Sotelo-Vazquez, C.; Abdul-Karim, N.; Maier, S. A.; Parkin, I. P., Photo-Induced Enhanced Raman Spectroscopy for Universal

Ultra-Trace Detection of Explosives, Pollutants and Biomolecules. *Nature Communications* **2016**, *7*.

3. Brongersma, M. L.; Halas, N. J.; Nordlander, P., Plasmon-Induced Hot Carrier Science and Technology. *Nature Nanotechnology* **2015**, *10*, 25-34.

4. Langer, J., et al., Present and Future of Surface-Enhanced Raman Scattering. *ACS Nano* **2019**, *14*, 28-117.

5. Wang, D.; Guan, J.; Hu, J.; Bourgeois, M. R.; Odom, T. W., Manipulating Light–Matter Interactions in Plasmonic Nanoparticle Lattices. *Accounts of Chemical Research* **2019**, *52*, 2997-3007.

6. Ross, M. B.; Mirkin, C. A.; Schatz, G. C., Optical Properties of One-, Two-, and Three-Dimensional Arrays of Plasmonic Nanostructures. *The Journal of Physical Chemistry C* **2016**, *120*, 816-830.

7. Blaber, M. G.; Arnold, M. D.; Ford, M. J., A Review of the Optical Properties of Alloys and Intermetallics for Plasmonics. *Journal of Physics: Condensed Matter* **2010**, *22*.

8. West, P. R.; Ishii, S.; Naik, G. V.; Emani, N. K.; Shalaev, V. M.; Boltasseva, A., Searching for Better Plasmonic Materials. *Laser & Photonics Reviews* **2010**, *4*, 795-808.

9. Kanipe, K. N.; Chidester, P. P. F.; Stucky, G. D.; Meinhart, C. D.; Moskovits, M., Properly Structured, Any Metal Can Produce Intense Surface Enhanced Raman Spectra. *The Journal of Physical Chemistry C* **2017**, *121*, 14269-14273.

10. Bezerra, A. G.; Machado, T. N.; Woiski, T. D.; Turchetti, D. A.; Lenz, J. A.; Akcelrud, L.; Schreiner, W. H., Plasmonics and Sers Activity of Post-Transition Metal Nanoparticles. *Journal of Nanoparticle Research* **2018**, *20*.

11. Barulin, A.; Claude, J.-B.; Patra, S.; Bonod, N.; Wenger, J., Deep Ultraviolet Plasmonic Enhancement of Single Protein Autofluorescence in Zero-Mode Waveguides. *Nano Letters* **2019**, *19*, 7434-7442.

12. Chowdhury, M. H.; Ray, K.; Gray, S. K.; Pond, J.; Lakowicz, J. R., Aluminum Nanoparticles as Substrates for Metal-Enhanced Fluorescence in the Ultraviolet for the Label-Free Detection of Biomolecules. *Analytical Chemistry* **2009**, *81*, 1397-1403.

13. Sharma, B.; Cardinal, M. F.; Ross, M. B.; Zrimsek, A. B.; Bykov, S. V.; Punihaole, D.; Asher, S. A.; Schatz, G. C.; Van Duyne, R. P., Aluminum Film-over-Nanosphere Substrates for Deep-Uv Surface-Enhanced Resonance Raman Spectroscopy. *Nano Letters* **2016**, *16*, 7968-7973.

14. Jha, S. K.; Ahmed, Z.; Agio, M.; Ekinci, Y.; Löffler, J. F., Deep-Uv Surface-Enhanced Resonance Raman Scattering of Adenine on Aluminum Nanoparticle Arrays. *Journal of the American Chemical Society* **2012**, *134*, 1966-1969.

15. Blaber, M. G.; Henry, A.-I.; Bingham, J. M.; Schatz, G. C.; Van Duyne, R. P., Lspr Imaging of Silver Triangular Nanoprisms: Correlating Scattering with Structure Using Electrodynamics for Plasmon Lifetime Analysis. *The Journal of Physical Chemistry C* **2011**, *116*, 393-403.

16. Hartland, G. V., Optical Studies of Dynamics in Noble Metal Nanostructures. *Chemical Reviews* **2011**, *111*, 3858-3887.

17. Zorić, I.; Zäch, M.; Kasemo, B.; Langhammer, C., Gold, Platinum, and Aluminum Nanodisk Plasmons: Material Independence, Subradiance, and Damping Mechanisms. *ACS Nano* **2011**, *5*, 2535-2546.

18. Plasmonics in the Ultraviolet with Aluminum, Gallium, Magnesium and Rhodium. *Applied Sciences* **2018**, *8*.

19. Biggins, J. S.; Yazdi, S.; Ringe, E., Magnesium Nanoparticle Plasmonics. *Nano Letters* **2018**, *18*, 3752-3758.

20. Knight, M. W.; King, N. S.; Liu, L.; Everitt, H. O.; Nordlander, P.; Halas, N. J., Aluminum for Plasmonics. *ACS Nano* **2013**, *8*, 834-840.

21. McMahon, J. M.; Schatz, G. C.; Gray, S. K., Plasmonics in the Ultraviolet with the Poor Metals Al, Ga, in, Sn, Tl, Pb, and Bi. *Phys. Chem. Chem. Phys.* **2013**, *15*, 5415-5423.

22. Toudert, J.; Serna, R.; Camps, I.; Wojcik, J.; Mascher, P.; Rebollar, E.; Ezquerra, T. A., Unveiling the Far Infrared-to-Ultraviolet Optical Properties of Bismuth for Applications in Plasmonics and Nanophotonics. *The Journal of Physical Chemistry C* **2017**, *121*, 3511-3521.

23. Watson, A. M.; Zhang, X.; Alcaraz de la Osa, R.; Sanz, J. M.; González, F.; Moreno, F.; Finkelstein, G.; Liu, J.; Everitt, H. O., Rhodium Nanoparticles for Ultraviolet Plasmonics. *Nano Letters* **2015**, *15*, 1095-1100.

24. Yang, Y.; Callahan, J. M.; Kim, T.-H.; Brown, A. S.; Everitt, H. O., Ultraviolet Nanoplasmonics: A Demonstration of Surface-Enhanced Raman Spectroscopy, Fluorescence, and Photodegradation Using Gallium Nanoparticles. *Nano Letters* **2013**, *13*, 2837-2841.

25. Zeman, E. J.; Schatz, G. C., An Accurate Electromagnetic Theory Study of Surface Enhancement Factors for Silver, Gold, Copper, Lithium, Sodium, Aluminum, Gallium, Indium, Zinc, and Cadmium. *The Journal of Physical Chemistry* **2002**, *91*, 634-643.

26. Ostovar, B., et al., Acoustic Vibrations of Al Nanocrystals: Size, Shape, and Crystallinity Revealed by Single-Particle Transient Extinction Spectroscopy. *The Journal of Physical Chemistry A* **2020**, *124*, 3924-3934.

27. Ross, M. B.; Schatz, G. C., Radiative Effects in Plasmonic Aluminum and Silver Nanospheres and Nanorods. *Journal of Physics D: Applied Physics* **2015**, *48*.

28. Sobhani, A.; Manjavacas, A.; Cao, Y.; McClain, M. J.; García de Abajo, F. J.; Nordlander, P.; Halas, N. J., Pronounced Linewidth Narrowing of an Aluminum Nanoparticle Plasmon Resonance by Interaction with an Aluminum Metallic Film. *Nano Letters* **2015**, *15*, 6946-6951.

29. Su, M.-N., et al., Ultrafast Electron Dynamics in Single Aluminum Nanostructures. *Nano Letters* **2019**, *19*, 3091-3097.

30. Zhu, X.; Imran Hossain, G. M.; George, M.; Farhang, A.; Cicek, A.; Yanik, A. A., Beyond Noble Metals: High Q-Factor Aluminum Nanoplasmonics. *ACS Photonics* **2020**, *7*, 416-424.

31. Foerster, B.; Spata, V. A.; Carter, E. A.; Sönnichsen, C.; Link, S., Plasmon Damping Depends on the Chemical Nature of the Nanoparticle Interface. *Science Advances* **2019**, *5*.

32. Januar, M.; Liu, B.; Cheng, J.-C.; Hatanaka, K.; Misawa, H.; Hsiao, H.-H.; Liu, K.-C., Role of Depolarization Factors in the Evolution of a Dipolar Plasmonic Spectral Line in the Far- and near-Field Regimes. *The Journal of Physical Chemistry C* **2020**, *124*, 3250-3259.

33. Sönnichsen, C.; Franzl, T.; Wilk, T.; von Plessen, G.; Feldmann, J.; Wilson, O.; Mulvaney, P., Drastic Reduction of Plasmon Damping in Gold Nanorods. *Physical Review Letters* **2002**, *88*.

34. Linic, S.; Chavez, S.; Elias, R., Flow and Extraction of Energy and Charge Carriers in Hybrid Plasmonic Nanostructures. *Nature Materials* **2021**.

35. Mie, G., Beiträge Zur Optik Trüber Medien, Speziell Kolloidaler Metallösungen. *Annalen der Physik* **1908**, *330*, 377-445.

36. Johnson, P. B.; Christy, R. W., Optical Constants of the Noble Metals. *Physical Review B* **1972**, *6*, 4370-4379.

37. Palik, E. D.; Ghosh, G., *Handbook of Optical Constants of Solids*; Academic: Oralndo, FL, 1985.

38. Hunderi, O.; Ryberg, R., Band Structure and Optical Properties of Gallium. *Journal of Physics F: Metal Physics* **1974**, *4*, 2084-2095.

39. Jezequel, G.; Lemonnier, J. C.; Thomas, J., Optical Properties of Gallium Films between 2 and 15 Ev. *Journal of Physics F: Metal Physics* **1977**, *7*, 1613-1622.

40. Koyama, R. Y.; Smith, N. V.; Spicer, W. E., Optical Properties of Indium. *Physical Review B* **1973**, *8*, 2426-2432.

41. Liljenvall, H. G.; Mathewson, A. G.; Myers, H. P., The Optical Properties of Lead in the Energy Range 0·6-6 Ev. *Philosophical Magazine* **1970**, *22*, 243-253.

42. MacRae, R. A.; Arakawa, E. T.; Williams, M. W., Optical Properties of Vacuum-Evaporated White Tin. *Physical Review* **1967**, *162*, 615-620.

43. Ashcroft, N.W.; Mermin, N. D., *Solid State Physics*; Saunders College Publishing: New York, 1976.

44. Bohren, C. F.; Huffman, D. R., *Absorption and Scattering of Light by Small Particles*; Wiley: New York, 1983.

45. Rasskazov, I. L.; Zakomirnyi, V. I.; Utyushev, A. D.; Carney, P. S.; Moroz, A., Remarkable Predictive Power of the Modified Long Wavelength Approximation. *The Journal of Physical Chemistry C* **2021**, *125*, 1963-1971.

46. Sanz, J. M.; Ortiz, D.; Alcaraz de la Osa, R.; Saiz, J. M.; González, F.; Brown, A. S.; Losurdo, M.; Everitt, H. O.; Moreno, F., Uv Plasmonic Behavior of Various Metal Nanoparticles in the near- and Far-Field Regimes: Geometry and Substrate Effects. *The Journal of Physical Chemistry C* **2013**, *117*, 19606-19615.

47. Blaber, M. G.; Schatz, G. C., Extending Sers into the Infrared with Gold Nanosphere Dimers. *Chemical Communications* **2011**, *47*.

48. Chan, G. H.; Zhao, J.; Schatz, G. C.; Van Duyne, R. P., Localized Surface Plasmon Resonance Spectroscopy of Triangular Aluminum Nanoparticles. *The Journal of Physical Chemistry C* **2008**, *112*, 13958-13963.

49. Knight, M. W.; Liu, L.; Wang, Y.; Brown, L.; Mukherjee, S.; King, N. S.; Everitt, H. O.; Nordlander, P.; Halas, N. J., Aluminum Plasmonic Nanoantennas. *Nano Letters* **2012**, *12*, 6000-6004.

TOC Image